Liquid Crystalline and Light Emitting Polyacetylenes: Synthesis and Properties of Biphenyl-Containing Poly(1-alkynes) with Different Functional Bridges and Spacer Lengths

Jacky W. Y. Lam,[†] Yuping Dong,[†] Kevin K. L. Cheuk,[†] Jingdong Luo,[†] Zhiliang Xie,[†,‡] Hoi Sing Kwok,[‡] Zhishen Mo,[§] and Ben Zhong Tang*,[†,‡]

Department of Chemistry, Center for Display Research, Institute of Nano Science and Technology, and Open Laboratory of Chirotechnology of the Institute of Molecular Technology for Drug Discovery and Synthesis,[||] Hong Kong University of Science & Technology, Clear Water Bay, Kowloon, Hong Kong, China; and Laboratory of Polymer Physics, Changchun Institute of Applied Chemistry, Chinese Academy of Sciences, Changchun 130022, China

ABSTRACT: Biphenyl- (Biph-) containing 1-alkynes (**3** and **4**) and their polymers (**1** and **2**) with varying bridge groups and spacer lengths were synthesized and the effects of the structural variation on their properties, especially their mesomorphism and photoluminescence behaviors, were studied. The acetylene monomers **3**(3) [HC≡C(CH$_2$)$_3$O−Biph−OCO(CH$_2$)$_{10}$CH$_3$] and **4**(m) [HC≡C(CH$_2$)$_m$OCO−Biph−OCO(CH$_2$)$_{10}$-CH$_3$, $m = 3, 4$] were prepared by sequential etherization and esterification reactions of 1-alkynes. While **3**(3) exhibits enantiotropic crystal E and SmB mesophases, its structural cousin **4**(3) displays only a monotropic SmB phase. Enantiotropic SmA and SmB mesophases are, however, developed when the spacer length is increased to 4. Polymerizations of the monomers are effected by Mo-, W-, Rh-, and Fe-based catalysts, with the WCl$_6$−Ph$_4$Sn catalyst giving the best results (isolation yield up to 85% and M_w up to 59000). The polymers were characterized by IR, UV, NMR, TGA, DSC, POM, XRD, and PL analyses. Compared to **1**(3), **2**(3) shows a red-shifted absorption, a higher T_i, and a better packed interdigitated bilayer SmA$_d$ structure, while the mesophase of **2**(4) involves monolayer-packing arrangements of the mesogens. Upon photoexcitation, **1**(3) emits almost no light but **2**(m) gives a strong ultraviolet emission ($\lambda_{max} \sim 350$ nm), whose intensity increases with the spacer length.

Introduction

A wealth of side-chain liquid crystalline vinyl polymers has been synthesized and their structure−property relationships have been well evaluated.[1] In contrast, side-chain liquid crystalline acetylenic polymers have received little attention.[2] Akagi and Shirakawa[3] and Nuyken[4] have synthesized some liquid crystalline polyacetylenes, whose mesogenic pendants are, however, attached to the polymer backbones all through an ether-functional bridge. The limitation in the variety of the liquid crystalline polyacetylenes has prevented systematic investigation of their structure−property relationships. Attracted by the potential of creating mesomorphic conjugated polymers with exotic electronic and optical properties, we have worked on the design and synthesis of new liquid crystalline polyacetylenes. Through elaborate synthetic efforts,[5] we generated a wide variety of mesogenic polyacetylenes with different molecular structures.[6] Contrary to the "general" belief that a rigid backbone would distort the packing alignments of mesogens, we found that the polyacetylene backbone could play an active role in guiding the orientation of the mesogenic pendants.[7] In our previous work, we studied the mesomorphic properties of a pair of polyacetylenes with different bridge orientations and spacer lengths and revealed that the structural variables affected the mesomorphism of the polymers to a considerable extent.[8] To collect more information and to gain further insights into how structural variations affect mesomorphic properties of liquid crystalline polyacetylenes, in this study, we investigated the effects of functional bridge and spacer length on the mesomorphism of another pair of polyacetylenes, that is, poly-(5-{[(4′-{[(undecyl)carbonyl]oxy})-4-biphenylyl]oxy}-1-pentyne) [**1**(3)] and poly[m-({[(4′-{[(undecyl)carbonyl]-oxy})-4-biphenylyl]carbonyl}oxy)-1-alkynes] [**2**(m); Chart 1].

Liquid crystals and light emitters are complementary in property; a polymer with the two electrooptical features (both liquid crystalline and light emitting) is of practical value, which may offer an array of exciting opportunities for high-tech innovations. Such a polymer, for example, may emit polarized light when aligned, which may be utilized for the construction of lighting and orientating layers in liquid crystal optical display devices, thus obviating the use of backlight lamps, polyimide films, and polarizing sheets. The color and brightness of the light emitted by the liquid crystalline polymer may be manipulated by external fields,[9] which may lead to the development of readily tunable electrochromic and optical switching systems. If the polymers can emit ultraviolet (UV) light, that will be even better, because the UV emitters can act as "color converters" to generate low-energy visible lights of any colors through interaction with appropriate phosphors.[10]

* To whom correspondence should be addressed (Department of Chemistry, Hong Kong University of Science & Technology). Telephone: +852-2358-7375. Fax: +852-2358-1594. E-mail: tangbenz@ust.hk.

† Department of Chemistry, Institute of Nano Science and Technology, and Open Laboratory of Chirotechnology of the Institute of Molecular Technology for Drug Discovery and Synthesis, Hong Kong University of Science & Technology.

‡ Center for Display Research, Hong Kong University of Science & Technology.

§ Laboratory of Polymer Physics, Changchun Institute of Applied Chemistry.

|| The University Grants Committee (Hong Kong) Area of Excellence Scheme.

Chart 1

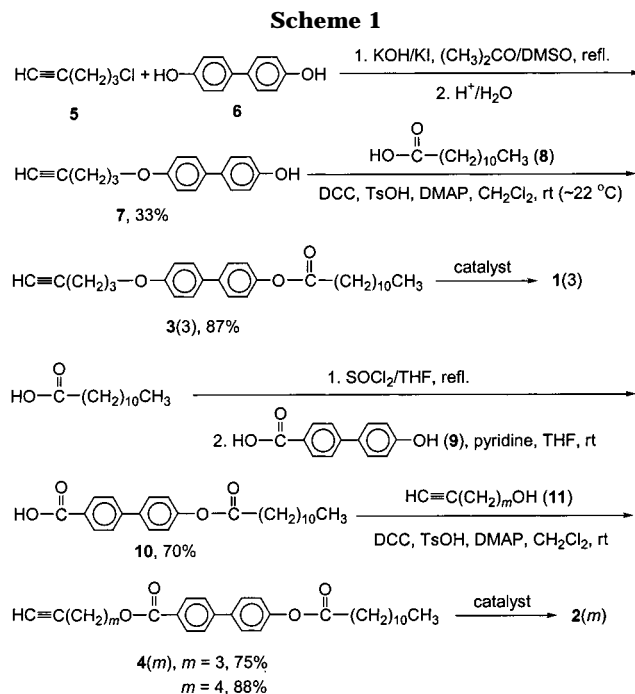**1**(3)   **2**(*m*) (*m* = 3, 4)

Scheme 1
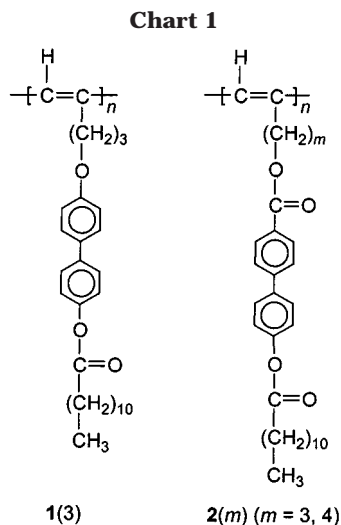
To develop such polymers, the first thing to learn is their structural requirements. Polyacetylenes have, however, "traditionally" been regarded as nonemissive polymers.[11] Recent studies have revealed that luminescence behaviors of polyacetylenes can be greatly tuned by changing their molecular structures. Whereas the (unsubstituted) polyacetylene $[-(CH=CH)_n-]$ is almost nonluminescent,[11] its disubstituted cousins $[-(CR=CR')_n-]$ can be strongly emissive.[12,13] Its monosubstituted derivatives of general structure $-[CH=C(Ar)]_n-$ or poly(1-arylacetylenes) are incapable of emitting intense light,[12-14] but chromophore-containing poly(1-alkylacetylene) or poly(1-alkynes) $\{-[CH=C(C_mH_{2m+1}-Ch)]_n-$; Ch, light-emitting chromophore} can be highly luminescent.[14] The mesogenic polymers **1**(3) and **2**(*m*) are monosubstituted derivatives of polyacetylene, and it is of interest to check how the molecular structures alter their light emitting behaviors. In this work, we examined their luminescence properties and found that the polymer with an ether bridge [**1**(3)] was nonluminescent but its counterpart with an ester bridge and a longer methylene spacer [**3**(4)] emitted strong UV light, whose intensity is comparable to that of poly(1-phenyl-1-octyne) (PPO), a highly luminescent disubstituted polyacetylene.[12,13]

Results and Discussion

Synthesis and Mesomorphism of Monomers. We synthesized the acetylene monomer 5-{[(4′-{[(undecyl)-carbonyl]oxy})-4-biphenylyl]oxy}-1-pentyne [**3**(3)] through a two-step reaction route. We first etherized 4′,4-biphenol with 5-chloro-1-pentyne, and the resulting alcohol (**7**) was then reacted with lauric acid in the presence of 1,3-dicyclohexylcarbodiimine (DCC), *p*-toluenesulfonic acid (TsOH), and 4-(dimethylamino)pyridine (DMAP) (Scheme 1). We also prepared *m*-({[(4′-{[(undecyl)carbonyl]oxy})-4-biphenylyl]carbonyl}oxy)-1-alkynes [**4**(*m*), *m* = 3, 4], which are the structural cousins of **3**(3) with a different functional bridge group (ester), through two consecutive esterification of 4′-hydroxy-4-biphenylcarboxylic acid (**9**). All the final products (monomers) were isolated in high yields (75−88%) and were fully characterized by spectroscopic methods, from which, satisfactory analysis data were obtained (see Experimental Section for details).

All the acetylene monomers are white crystals at room temperature and exhibit liquid crystallinity at elevated temperatures. The thermal transition behaviors of the monomers are examined by differential scanning calorimetry (DSC) and polarized optical microscopy (POM). Figure 1 shows the DSC thermograms of the monomers, while the POM textures of **3**(3) and **4**(*m*) observed on cooling from their isotropic states are given in Figure 2.

The first cooling scan of **3**(3) shows two sharp peaks at 113.9 and 47.0 °C (Figure 1A). POM observation reveals that upon cooling **3**(3) from the isotropic state
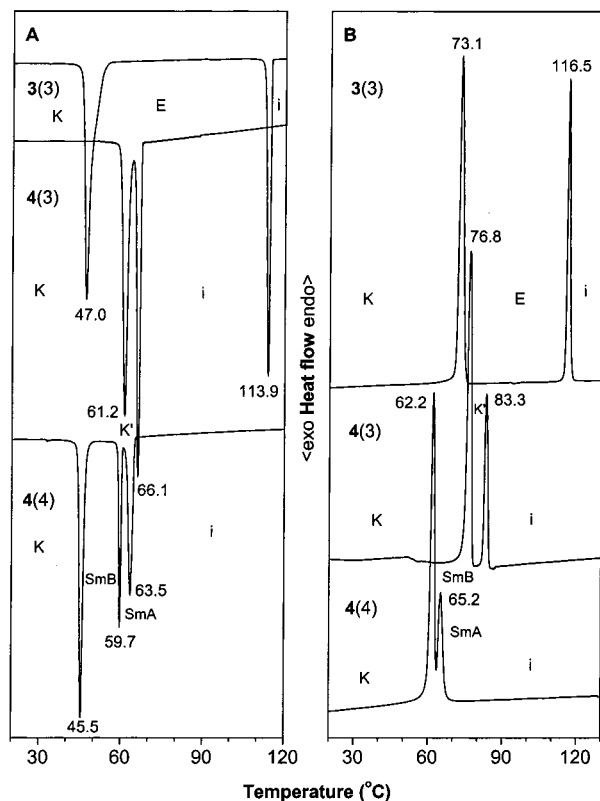

Figure 1. DSC thermograms of monomers **3**(3) and **4**(*m*) (*m* = 3, 4) recorded under nitrogen during the (A) first cooling and (B) second heating scans at a scan rate of 10 °C/min.
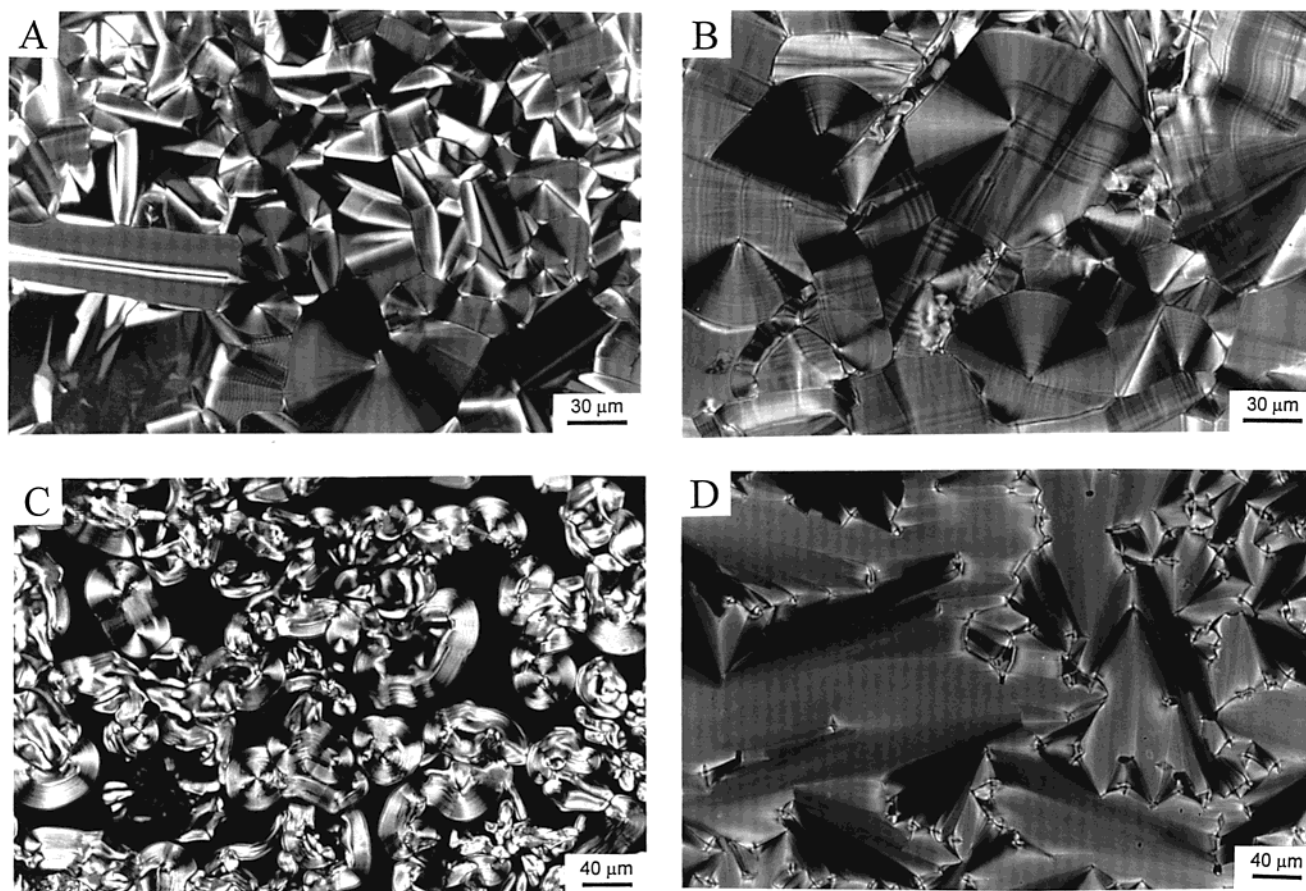
Figure 2. Polarized optical microphotographs of **3**(3) at (A) 114 °C (mosaic SmB texture with lancet) and (B) 110 °C (paramorphotic arced mosaic texture of crystal E phase), (C) **4**(3) at 66.2 °C (mosaic texture of SmB phase with pseudo π-disclination), and (D) **4**(4) at 59.0 °C (mosaic SmB texture).

to 114 °C, mosaic texture of SmB mesophase with lancet[15] is formed (Figure 2A). It is, however, difficult to identify whether **3**(3) enters hexatic or crystal SmB mesophases because the mosaic textures displayed by the two phases are indistinguishable.[15a] When the temperature is further lowered to 110 °C, *continuous concentric arcs* running across the backs of the mosaics are observed (Figure 2B). Of the different mesophases evolved from SmB phase, this paramorphotic arced mosaic texture can only be found in crystal E and G phases. The arcs in crystal G phase are, however, not continuous from one area to another and show breaks. It thus becomes clear that the crystal E phase has formed at 110 °C, formation of whose arcs is probably caused by the contraction of the layer ordering at the SmB−E transition.[15] The monomer solidifies at 47 °C. The crystal−E and E−liquid transitions are enantiotropic as the DSC thermogram recorded in the second heating scan displays two peaks at 73.1 and 116.5 °C.

Monomer **4**(3) structurally resembles **3**(3) but has a different functional bridge and it is of interest to study how it behaves mesomorphically. During the first cooling cycle, **4**(3) shows two transition peaks at 66.1 and 61.2 °C (Figure 1A). When **4**(3) is allowed to cool from the isotropic state to 66.2 °C, mosaic texture of the SmB phase with pseudo π-disclination[15b] is observed (Figure 2C). The temperature range of the mesophase is, however, narrow ($\sim$0.5 °C), and the monomer completely solidifies at 65.5 °C. The exothermic peak at 61.2 °C may thus be associated with crystal transformation from one state to another (k−k transition). The second heating scan records two transition peaks at 76.8 and

83.3 °C but no liquid crystalline texture is observed, indicating that the mesomorphism is monotropic.

The DSC thermogram of **4**(4) shows three transition peaks at 63.5, 59.7, and 45.5 °C in the first cooling cycle (Figure 1A). The mesophase in this temperature range (63.5−59.7 °C) is identified to be SmA because typical focal−conic fan texture is observed when **4**(4) is cooled to 63.0 °C. The radical lines running across the backs of the fans, however, disappear upon further cooling to 59.0 °C. Annealing the texture at the same temperature for 10 minutes results in the formation of mosaic texture of SmB phase (Figure 2D). Since no transition bars are observed during the SmA−SmB transition, the mesophase formed by **4**(4) is thus hexatic in nature.[15a] The monomer solidifies at 44.0 °C. Reheating **4**(4) regenerates the SmB and SmA textures in sequence; that is, the mesomorphism is enantiotropic.

Table 1 summarizes the thermal transitions and the corresponding thermodynamic parameters of the acetylene monomers. All the SmA, SmB, and crystal E transitions involve large enthalpy (ΔH) and entropy (ΔS) changes. These suggest that all the transitions are first order in nature.[15c,16] Although the change in the functional bridge looks like a subtle structural variation, it does change the mesomorphic properties of the acetylene monomers to a great extent, with **3**(3) exhibiting better packing order and higher transition temperatures. The melting temperature of **4**(4) is lower than that of **4**(3), probably due to the plasticization effect of the longer methylene spacers.

Polymerization Reactions. Since Akagi and Shirakwa polymerized their mesogenic monomers such as

Table 1. Thermal Transitions and Corresponding Thermodynamic Parameters of 3(3) and 4(*m*)[a]

		T, °C [ΔH, kJ/mol; ΔS, J/(mol K)]	
no.	monomer	cooling	heating
1	**3**(3)	i 113.9 (−19.34; −49.97)[b] E 47.0 (−32.81; −102.49) k	k 73.1 (41.32; 119.34)[b] E 116.5 (25.21; 64.7) i
2	**4**(3)	i 66.1 (−14.56; −42.92)[b] k′ 51.2 (−16.99; −52.38) k	k 76.8 (28.32; 80.93) k′ 83.3 (11.67; 33.21) i
3	**4**(4)	i 63.5 (−9.67; −28.73) SmA 59.7 (−5.86; −17.61) SmB 45.5 (−6.71; −21.06) k	k 62.2 (19.0; 56.6)[b] SmA 65.2 (5.61; 16.58) i

[a] Data taken from the DSC thermograms recorded under nitrogen in the first cooling and second heating scans; abbreviations: k = crystalline state, Sm = smectic phase, i = isotropic state. [b] Sum of overalpping transitions.

Table 2. Polymerization of 5-{[(4′-{[(Undecyl)carbonyl]oxy})-4-biphenylyl]oxy}-1-pentyne [3(3)][a]

no.	catalyst[b]	solvent	temp[c] (°C)	yield (%)	M_w[d]	M_w/M_n[d]
1	MoCl$_5$−Ph$_4$Sn	toluene	rt	50.8	9770	1.72
2	[Rh(nbd)Cl]$_2$	Et$_3$N	60	92.3	4210	1.20
3	[Rh(nbd)Cl]$_2$	toluene/Et$_3$N[e]	rt	91.3	4300	1.26
4	Fe(acac)$_3$−3Et$_3$Al	dioxane	rt	59.7	3630	1.33
5	Fe(acac)$_3$−3Et$_3$Al	toluene	rt	60.3	4870	1.43
6	WCl$_6$−Ph$_4$Sn	toluene	rt	77.2	12900	2.07
7	WCl$_6$−Ph$_4$Sn	toluene	40	41.7	13500	2.18
8	WCl$_6$−Ph$_4$Sn	toluene	60	17.4	9750	1.78
9	WCl$_6$−Ph$_4$Sn	toluene	80	trace		
10	WCl$_6$−Ph$_4$Sn	dioxane	rt	68.9	18600	2.48
11	WCl$_6$−Ph$_4$Sn	dioxane	60	68.6	10800	2.16
12	WCl$_6$−Ph$_4$Sn	dioxane	80	80.7	12500	2.65
13	Mo(nbd)(CO)$_4$	CCl$_4$	60	36.7	12700	1.67
14	W(mes)(CO)$_3$	CCl$_4$	60	64.0	15700	1.73

[a] Carried out under nitrogen for 24 h; [M]$_0$ = 0.2 M; [cat.] = ([cocat.] =) 10 mM; for Zielger−Natta catalyst, [AlEt$_3$] = 3[Fe-(acac)$_3$]. [b] Abbreviations: mes = mesitylene, nbd = 2,5-norborn-diene, and acac = acetylacetonate. [c] rt = room temperature. [d] Determined by GPC in THF on the basis of a polystyrene calibration. [e] Volume ratio of toluene to Et$_3$N = 4:1.

Table 3. Polymerization of 5-({[(4′-{[(Undecyl)carbonyl]oxy})-4-biphenylyl]carbonyl}oxy)-1-pentyne [4(3)][a]

no.	catalyst	solvent	temp[b] (°C)	yield (%)	M_w[c]	M_w/M_n[c]
1	MoCl$_5$−Ph$_4$Sn	dioxane	rt	7.4	33000	2.02
2	WCl$_6$−Ph$_4$Sn	dioxane	rt	21.4	47400	2.01
3	WCl$_6$−Ph$_4$Sn	dioxane	60	84.1	37700	1.90
4	WCl$_6$−Ph$_4$Sn	toluene	rt	84.7	52900	1.95

[a] Carried out under nitrogen for 24 h; [M]$_0$ = 0.2 M; [cat.] = ([cocat.] =) 10 mM. [b] rt = room temperature. [c] Determined by GPC in THF on the basis of a polystyrene calibration.

Table 4. Polymerization of 6-({[(4′-{[(Undecyl)carbonyl]oxy})-4-biphenylyl]carbonyl}oxy)-1-hexyne [4(4)][a]

no.	catalyst[b]	solvent	temp[c] (°C)	yield (%)	M_w[d]	M_w/M_n[d]
1	MoCl$_5$−Ph$_4$Sn	dioxane	rt	10.8	33500	1.97
2	WCl$_6$−Ph$_4$Sn	dioxane	rt	26.5	71200	2.16
3	WCl$_6$−Ph$_4$Sn	dioxane	60	82.3	59000	1.85
4	WCl$_6$−Ph$_4$Sn	toluene	rt	15.9	53600	2.07
5	Mo(nbd)(CO)$_3$	CCl$_4$	60	40.6	13300	1.44
6	W(mes)(CO)$_4$	CCl$_4$	60	52.1	17100	1.62

[a] Carried out under nitrogen for 24 h; [M]$_0$ = 0.2 M; [cat.] = ([cocat.] =) 10 mM. [b] Abbreviations: mes = mesitylene and nbd = 2,5-norborndiene. [c] rt = room temperature. [d] Determined by GPC in THF on the basis of a polystyrene calibration.

5-[(4′-pentyl-4-biphenylyl)oxy]-1-pentyne [HC≡C(CH$_2$)$_3$−Biph−C$_5$H$_{11}$] by MoCl$_5$−Ph$_4$Sn, [Rh(nbd)Cl]$_2$, and Fe-(acac)$_3$−3Et$_3$Al catalysts,[3] we checked whether these catalysts were also effective for the polymerization of **3**(3). MoCl$_5$−Ph$_4$Sn initiates the polymerization of **3**(3) in toluene, giving 51% of a polymeric product with a molecular weight of 9770 (Table 2, no. 1). [Rh(nbd)Cl]$_2$ produces a polymer in 92% yield, whose molecular weight is, however, low. No increase in the molecular weight is observed when the polymerization is conducted in a mixture of toluene and Et$_3$N. Polymerizations of **3**(3) can also be achieved by Fe(acac)$_3$−3Et$_3$Al in toluene and dioxane, but the molecular weights of the polymers are again low, probably due to the poisoning interaction of the polar ester group with the catalyst. We have previously found that WCl$_6$−Ph$_4$Sn performs much better than MoCl$_5$−Ph$_4$Sn in the polymerizations of mesogen-containing acetylene monomers.[5] Under similar conditions, polymerization of **3**(3) in toluene catalyzed by WCl$_6$−Ph$_4$Sn gives a comparatively high molecular weight polymer in a high yield. In this solvent, raising the temperature leads to decreases of both molecular weight and yield, probably due to instability of the catalytic species and/or activation of termination reactions. Dioxane is also a good solvent for the polymerization. Unlike the trend observed in toluene, the polymer yield and M_w are less sensitive to the change in temperature; complexation of the polar solvent molecule(s) of dioxane with the metal center may have generated a more stable tungsten−oxo catalytic center, which may be resistant to the attach of detrimental terminators.[5c] W(mes)(CO)$_3$ and Mo(nbd)(CO)$_4$ are air- and moisture-stable metal carbonyl complexes and can polymerize acetylenes in both halogenated and nonhalogenated solvents.[5] Both W(mes)(CO)$_3$ and Mo-(nbd)(CO)$_4$ effect polymerization of **3**(3) in carbon tetrachloride, with the latter producing a higher molecular weight polymer in a higher yield.

Unlike **3**(3), **4**(3) cannot be effectively polymerized by MoCl$_5$−Ph$_4$Sn (Table 3, no. 1). WCl$_6$−Ph$_4$Sn, on the other hand, performs much better under similar conditions. The yield is greatly boosted when temperature is raised to 60 °C. Toluene is generally a poorer solvent than dioxane in the polymerizations of functional acetylene monomers at high temperatures.[5c] But at low temperatures, the solvent is not "bad": a high molecular weight polymer is obtained in a high yield when the polymerization of **4**(3) is carried out in toluene at room temperature.

Similar to **4**(3), **4**(4) undergoes sluggish polymerization when MoCl$_5$−Ph$_4$Sn is used as the catalyst in dioxane (Table 4, no. 1). Both the yield and molecular weight are increased when the catalyst is changed to WCl$_6$−Ph$_4$Sn. Although the molecular weight of the polymer drops, the yield increases more than three times when the polymerization is performed at 60 °C. Surprisingly, polymerization of **4**(4) in toluene only gives 15.9% of a polymeric product although it is a good solvent for the polymerization of **4**(3). The reason for this is unclear at present but will be investigated in the future. The metal carbonyl catalysts Mo(nbd)(CO)$_3$ and W(mes)(CO)$_4$ are effective for the polymerization of **4**(4), giving polymers in moderate yields with narrow polydispersities.
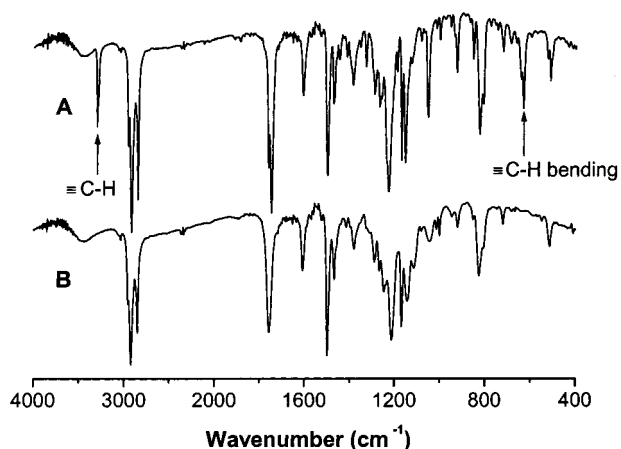
Figure 3. IR spectra of (A) **3**(3) and (B) its polymer **1**(3) (sample taken from Table 2, no. 11).
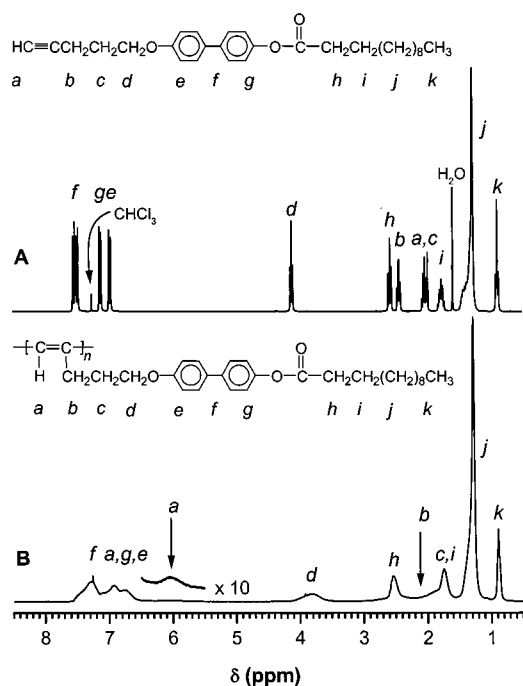

Figure 4. ^{1}H NMR spectra of (A) **3**(3) and (B) its polymer **1**(3) (sample from Table 2, no. 11).

Figure 5. ^{13}C NMR spectra of **3**(3) and its polymer **1**(3) (sample from Table 2, no. 11).

at δ 6.05.[17] It thus seems reasonable to assign the peak centered at δ 6.04 to the absorption by the cis olefin proton in the alternating double-bond backbone of **1**(3). The cis content of the polymer can be calculated according to[5–8]

$$\text{cis content (\%)} = [A_{\text{cis}}/(A_{\text{total}}/9)] \times 100 \qquad (1)$$

where A_{cis} and A_{total} are respectively the integrated peak areas of the absorption by the cis olefin proton and of the total absorption by the aromatic and olefinic protons. Using eq 1, the cis content of **1**(3) is calculated to be 45% (or 55% trans). The polymer thus consists of comparable amounts of cis and trans stereoisomers, as evidenced by its relatively broad absorption peaks.

Figure 5 shows the ^{13}C NMR spectrum of **3**(3) along with that of its polymer **1**(3). While the acetylene carbon atoms of **3**(3) absorb at δ 83.3 and 66.1, these absorptions disappear in the spectrum of **1**(3). The absorption of the propargyl carbon of **3**(3) at δ 15.1 also disappears owing to its transformation to the allylic structure in **1**(3) by the acetylene polymerization. The absorptions of the olefin carbon atoms of the backbone are, however, not distinguishable because of their overlapping with the peaks of the carbon atoms of the aromatic pendants.

The UV absorption spectra of chloroform solutions of the polymers are given in Figure 6. None of the monomers shows any peaks at wavelengths longer than 325 nm; the absorption in the long-wavelength visible spectral region is thus obviously from the double-bond

Structural Characterization. All the purified polymerization products give satisfactory spectroscopic data corresponding to their expected molecular structures (see Experimental Section for details). An example of the IR spectrum of **1**(3) is given in Figure 3. The spectrum of its monomer **3**(3) is also shown in the same figure for comparison. The $\equiv$C−H stretching and bending vibrations of the monomer are observed at 3200 and 630 cm^{-1}. All these acetylene absorption bands disappear in the spectrum of its polymer, indicating that the triple bonds have been consumed by the polymerization reaction.

NMR analysis proves that the acetylene triple bonds have been transformed to polyene double bonds. Figure 4 shows the ^{1}H NMR spectra of **3**(3) and its polymer **1**(3) in chloroform. There is no peak in the acetylene absorption region ($\delta \sim 2.0$) in the spectrum of the polymer. Instead, a new broad peak appears in the olefin absorption region (δ 6.5−5.8). Masuda and Higashimura have reported that the cis olefin proton of an aliphatic poly(1-alkyne), poly(3,3-dimethyl-1-pentyne), absorbs
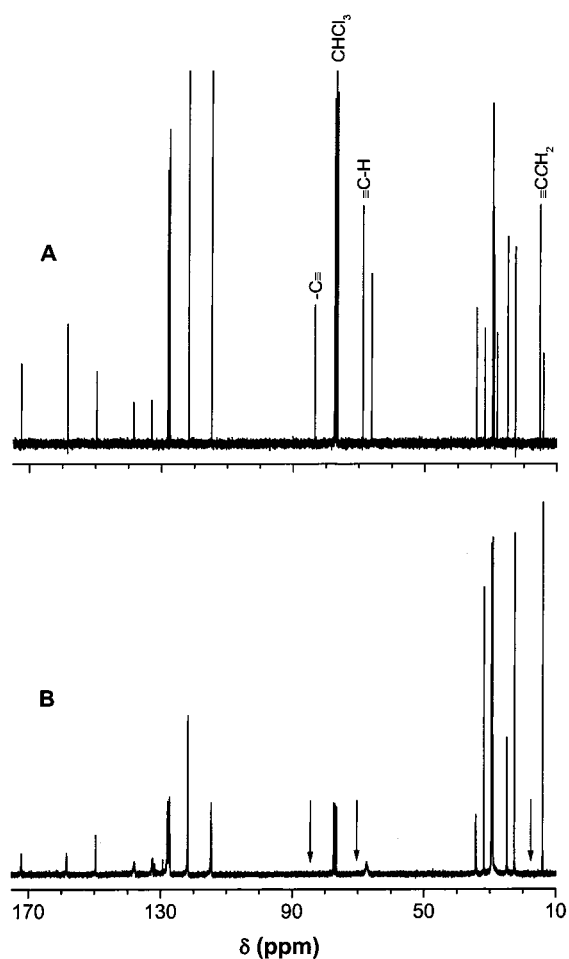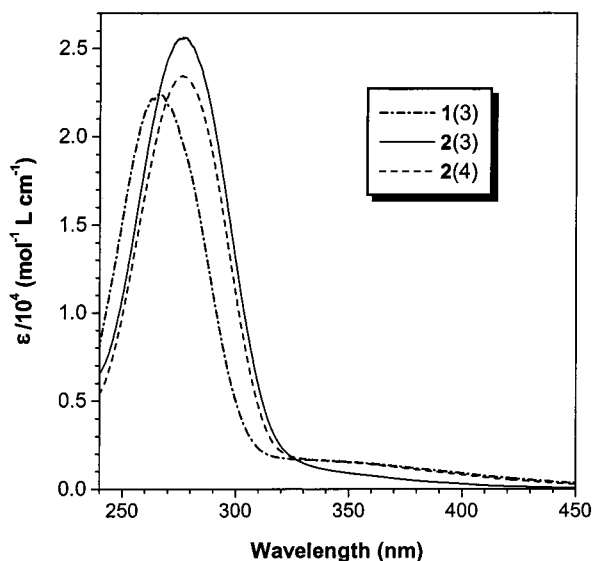
Figure 6. UV spectra of chloroform solutions of **1**(3) (sample from Table, 2, no. 11), **2**(3) (Table 3, no. 3), and **2**(4) (Table 4, no. 3).

Figure 7. TGA thermograms of **1**(3) (sample from Table 2, no. 11), **2**(3) (Table 3, no. 3), **2**(4) (Table 4, no. 3), and poly(1-hexyne) (PH; data taken from ref 18b) recorded under nitrogen at a heating rate of 10 °C/min.

backbones of the polymers. The absorptivity is low, probably owing to the reduction of the effective conjugation lengths along the polyacetylene backbone by the bulky pendant groups. The undecylcarbonyloxybiphenylyloxy pendants of **1**(3) absorb at 265 nm, which is ~12 nm blue-shifted from those of **2**(*m*). The biphenylyl chromphores of **2**(*m*) are well polarized by the push–pull interaction of the electron-donating undecylcarbonyloxy and electron-withdrawing carbonyloxy groups.[8] The polarizability of the pendants in **1**(3) is, however, low because both undecylcarbonyloxy and ether groups are electron-donating.

Stability, Mesomorphism, and Luminescence. Since the formation of mesophases of a thermotropic liquid crystalline polymer is realized by the application of heat, the thermal stability of the polymer is thus of primary importance. Poly(1-hexyne) (PH), which may be regarded as the parent form of the mesogen-containing poly(1-alkynes), is so unstable that it starts to lose its weight at ~150 °C (Figure 7; with the starting M_w and M_w/M_n of PH being 410 000 and 3.2, respectively).[18] On the other hand, all the mesogenic polyacetylenes almost do not lose any weights at a temperature as high as ~300 °C. Clearly, the introduction of the mesogenic units into the macromolecular structures has dramatically enhanced the resistance of the polymers to thermolysis, probably due to the protective "jacket effect" of the thermally stable mesogenic pendants.[6–8] The thermal stability of the polymers is further substantiated by the DSC analysis: no irreversible peaks suspiciously associated with polymer degradation are observed at the high temperatures during the cycles of repeated heating–cooling scans.

After confirming the stability of the polymers by the thermal analyses, we studied their mesomorphic properties. Figure 8 shows the DSC thermograms of **1**(3) and **2**(*m*) recorded under nitrogen during the first cooling and second heating scans. In the first cooling cycle, a broad exothermic peak associated with i–SmA is observed at 121.5 °C in **1**(3) and the corresponding SmA–i transition is detected at 137.7 °C. Polymer **2**(3) enters the SmA phase from its isotropic state at 198.8 °C. The mesophase is stable in a temperature range over 48 °C before **2**(3) finally solidifies at 150.3 °C. The associated
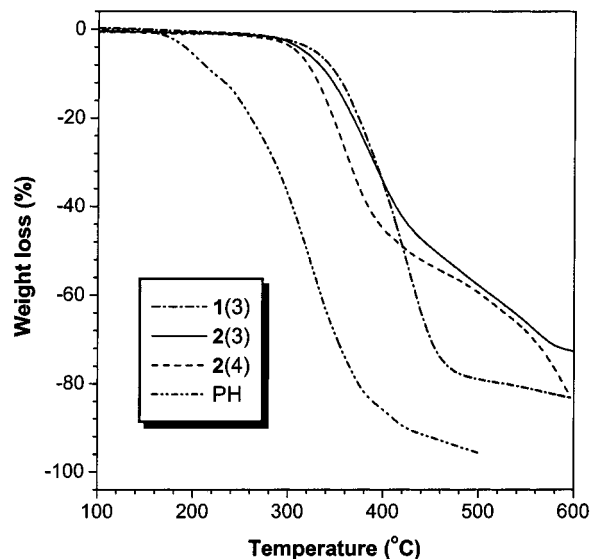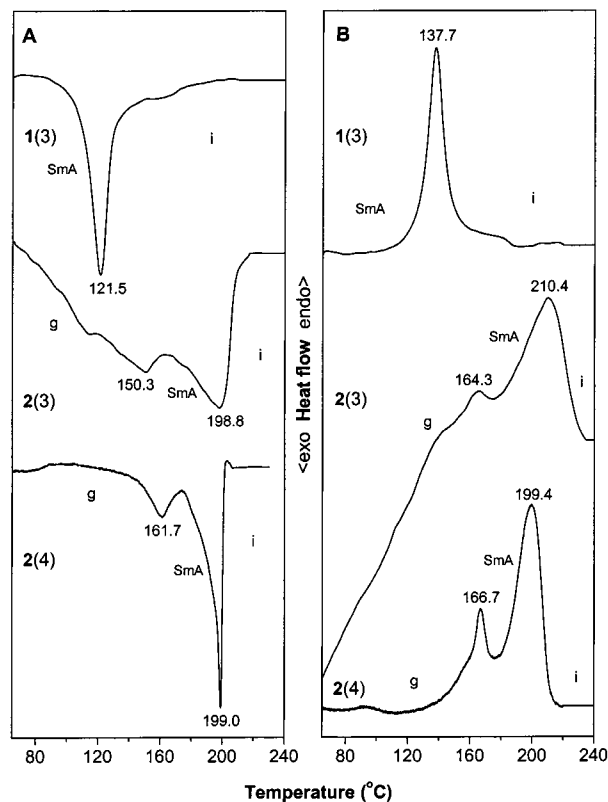

Figure 8. DSC thermograms of the mesomorphic poly(1-alkynes) **1**(3) (sample from Table 2, no. 11), **2**(3) (Table 3, no. 3), and **2**(4) (Table 4, no. 3) recorded under nitrogen during the (A) first cooling and (B) second heating scans at a scan rate of 10 °C/min.

g–SmA and SmA–i transitions are observed at 164.3 and 210.4 °C. The transition profiles of **2**(4) are similar to those of **2**(3) and i–SmA and SmA–g transitions are found at 199.0 and 161.7 °C. Peaks corresponding to g–SmA and SmA–i transitions are observed at 199.4 and 166.7 °C.

Figure 9 shows the POM microphotographs of the mesomorphic textures of **1**(3) and **2**(*m*). When **1**(3) is cooled from its isotropic state, small anisotropic rhombic
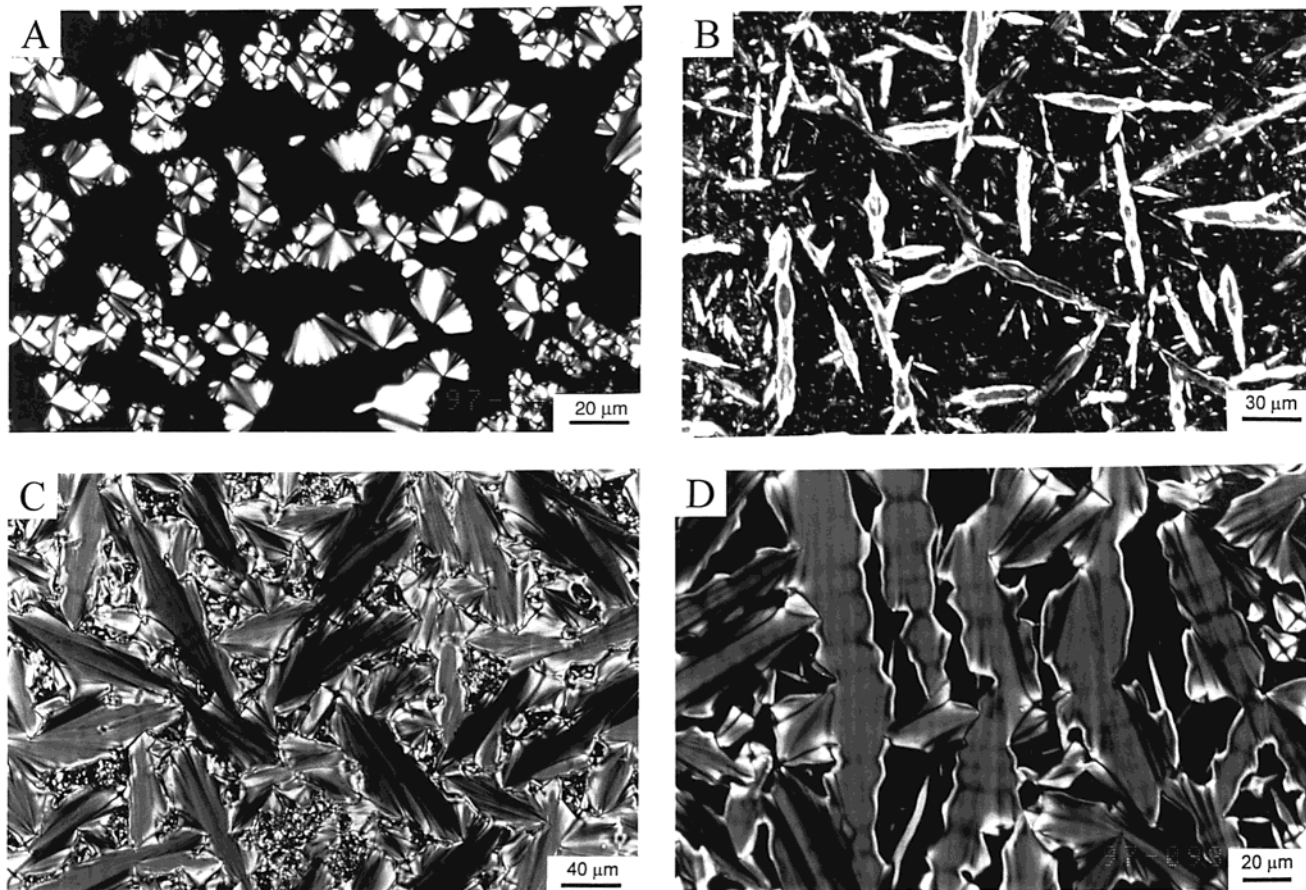
Figure 9. Mesomorphic textures observed on cooling (A) **1**(3) (sample from Table 2, no. 11) to 165 °C, **2**(3) (Table 3, no. 3) (B) to 200 and (C) 170 °C, and (D) **2**(4) (Table 4, no. 3) to 160 °C from their isotropic melts.

Table 5. Thermal Transitions and Corresponding Thermodynamic Parameters of 1(3) and 2(*m*)[a]

		T, °C [ΔH, kJ/mru; ΔS, J/(mru K)][b]	
no.	polymer	cooling	heating
1	**1**(3)	i 121.5 (−6.86; −17.38) SmA	SmA 137.7 (6.56; 15.97) i
2	**2**(3)	i 198.8 (−2.52; −5.34) SmA 150.3 (−0.30; −0.71) g	g 164.3 (0.20; 0.46) SmA 210.4 (3.09; 6.39) i
3	**2**(4)	i 199.0 (−3.71; −7.84) SmA 161.3 (−0.78; −1.80) g	g 166.7 (0.38; 0.86) SmA 199.4 (3.77; 7.98) i

[a] Data taken from the DSC thermograms recorded under dry nitrogen in the first cooling and second heating scans. Abbreviations: k = crystalline state, Sm = smectic phase, g = glassy state, and i = isotropic liquid. [b] Abbreviation: mru = monomer repeat unit.

entities emerge from the dark background of the isotropic liquid. The fine textures grow into fanlike structures upon further cooling (Figure 9A) but the exact nature of the mesophase is difficult to identify. We repeatedly tried to grow the liquid crystals with care but failed to obtain any readily identifiable characteristic textures. With the aid of X-ray diffraction (XRD) measurements, the textures are identified to be associated with a SmA phase (see below).

Polymer **2**(3), however, exhibits typical SmA textures in the mesomorphic temperature region. When **2**(3) is cooled from the isotropic state to 200 °C, many small bâtonnets appear. The bâtonnets grow to bigger domains when the sample is further cooled. Interestingly, inside the layer, parallel bands normal to the director of the bâtonnets are clearly seen (Figure 9B). Such banded textures have often been observed in other liquid crystalline polyacetylenes that form SmA mesophase,[6−8] suggesting that it is a common phenomenon observable in smectic polyacetylene systems. Further lowering the temperature encourages further growth of the bâtonnets. Coalescence of the anisotropic domains results in the formation of well-developed characteristic focal−

conic fan texture (Figure 9C). The banded textures observed in the early stage of the mesomorphic transition are, however, completely buried. The mesomorphic textures formed in **2**(4) are similar to those of **2**(3) and as shown in Figure 9D, very large bâtonnets with banded textures are also observed upon cooling the isotropic liquid of **2**(4).

The thermal transitions and their corresponding enthalpy and entropy changes of **1**(3) and **2**(*m*) are summarized in Table 5. The large ΔH and ΔS changes involved in the mesomorphic transitions of **1**(3) and **2**(*m*) rule out the possibility of nematic phase and further support the assignment of smecticity to the mesophases of the polyacetylene liquid crystals. It is of interest to note that the polymer having an ester-functional bridge [**2**(3)] shows higher T_i than the one with an ether bridge [**1**(3)] ($\Delta T \sim 77$ °C), in agreement with the POM observation that **2**(3) displays better developed mesomorphic textures. On the other hand, the change in spacer length [**2**(3) vs **2**(4)] has little influence on the T_i of the polymers.

We carried out powder XRD experiments in order to gain more information concerning the molecular ar-
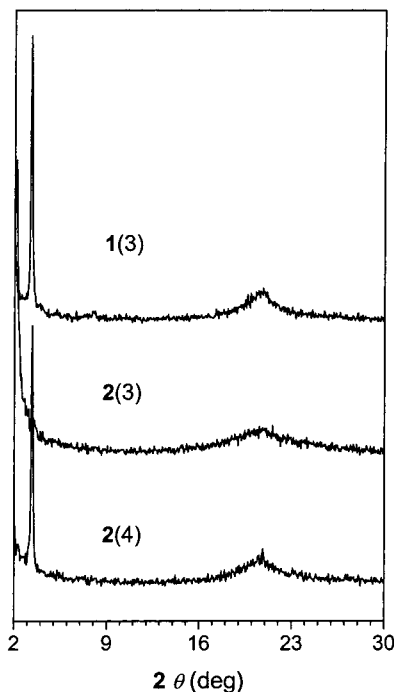
Figure 10. X-ray diffraction patterns of the mesogenic polyacetylenes quenched with liquid nitrogen from their liquid crystalline states: **1**(3) (sample from Table 2, no. 11) at 150 °C, **2**(3) (Table 3, no. 3), and **2**(4) (Tables 4, no. 3) at 170 °C.

Table 6. X-ray Diffraction Analysis Data of 1(3) and 2(m)^a

polymer	T (°C)	d_1 (Å)	d_2 (Å)	molecular length (l, Å)^b	ratio d_1/l	phase
1(3)	150	27.16	4.26	28.36	0.96	SmA
2(3)	170	41.06	4.27	30.21	1.36	SmA$_d$
2(4)	170	26.35	4.26	31.46	0.84	SmA

^{a} The mesophases in the liquid crystalline states at the given temperatures were frozen by the rapid quenching with liquid nitrogen. ^{b} Calculated from the monomer repeat units in their fully extended conformation.

rangements, modes of packing, and types of order in the mesophases of the polyacetylene liquid crystals. The diffractogram of **1**(3) shows a sharp reflection and a broad halo at $2\theta = 3.25$ and $20.85°$, respectively, from which d spacings of 27.16 and 4.26 Å are derived (Figure 10). The existence of long-range positional order in the polymer again rules out the possibility of nematic classification.[19] The calculated molecular length of one monomer repeat unit (mru) of **1**(3) is 28.36 Å, which is close to the experimentally obtained layer thickness (Table 6). This confirms the SmA nature of the mesophase and suggests that the mesogens are packed in a monolayer structure.

The XRD diffractogram of **2**(3) also displays Bragg reflections at low and middle angles. The sharp reflection at the low angle ($2\theta = 2.15°$) corresponds to a layer spacing of 41.06 Å, which is in considerable excess of the molecular length (30.21 Å). The mesophase in **2**(3) thus involves a bilayer packing arrangement, in which the alkoxy tails are interdigitated in an antiparallel fashion.[5c,8] Interestingly, when the spacer length is increased by one methylene unit, **2**(4) forms SmA mesophase of a monolayer structure. Clearly, the type of the functional bridge and length of the methylene spacer dramatically affect the layer structure of the liquid crystalline polyacetylenes.

Previous studies by us[14] and others[12,13] have revealed that light-emitting efficiencies of monosubstituted poly-
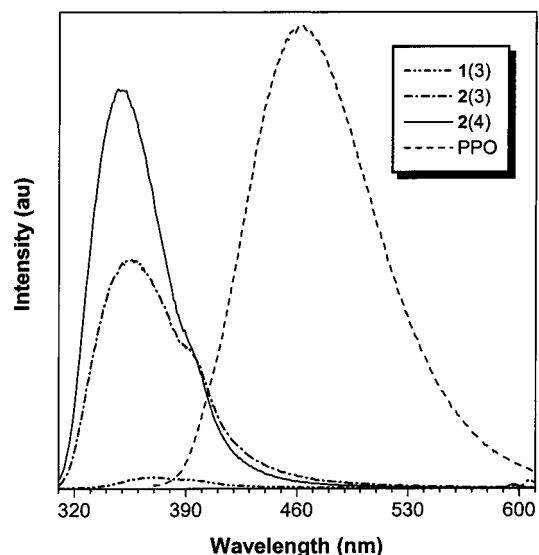

Figure 11. Photoluminescence spectra of chloroform solutions of **1**(3) (sample from Table 2, no. 11), **2**(3) (Table 3, no. 3), **2**(4) (Table 4, no. 3), and poly(1-phenyl-1-octyne) (PPO). Concentration: 0.05 mM. Excitation wavelengths (nm): 320 [**1**(3)], 315 [**2**(3) and **2**(4)], and 350 (PPO).

acetylenes are sensitive to their molecular structures. Will the structural variations of functional bridge and spacer length affect the luminescence behaviors of the liquid crystalline poly(1-alkynes)? The answer is a firm yes: While a weak emission peaked at 370 nm is observed when **1**(3) is photoexcited at 320 nm (Figure 11), **2**(3) emits a strong UV light of 353 nm, whose intensity is ~20 times higher than that from **1**(3). Polymer **2**(4) emits even more strongly at 347 nm and its luminescence intensity is comparable to that of PPO, a well-known highly fluorescent disubstituted polyacetylene.[12,13]

Whereas the emission of PPO at 460 nm is by the polyarylalkyne backbone,[12,13] we have previously clearly demonstrated that the polyene backbone of a poly(1-alkyne) emits faintly in the red spectral region with a λ_{max} of ~740 nm.[14b] The UV light emitting by polymers **1** and **2** thus must be from their pendant chromophores. The pendants of **1**(3) are not good lumophores because of their unfavorable electronic structures, as discussed above (cf., Figure 6). On the other hand, the chromophoric pendants in **2**(3) are well polarized by the electron-donating and -withdrawing groups. This push–pull interaction increases the mobility of the π-electrons, thus leading to the enhanced emission. The increase of emission intensity with the spacer length in the series of **2**(m) is in agreement with the observations of Yoshino[12] and Kabayashi,[13] who have found that longer alkyl chains favor stronger emission in the photoluminescence and electroluminescence of poly(1-phenyl-1-alkynes). The longer alkyl chains may have better segregated the chromophoric pendants, which effectively hampers the excitons from traveling to the quenching sites of the polyacetylene backbone and hence enhances the chances for the confined excitons to recombine radiatively.[12,13]

Conclusions

In this work, the mesogenic and chromophoric acetylene monomers and polymers with different functional bridges and spacer lengths are designed and synthesized. The structural variations on the chemical and

physical properties of the monomers and polymers are investigated and the results can be summarized as follows:

(1) All the acetylene monomers **3**(3) and **4**(*m*) are liquid crystalline, and the monomer with the ether-functional bridge shows better ordered mesophase and higher transition temperatures than its counterpart with the ester-functional bridge.

(2) WCl₆−Ph₄Sn and MoCl₅−Ph₄Sn catalysts are good at polymerizing **3**(3) in toluene and dioxane. For **4**(*m*), the best polymerization results are obtained in dioxane using WCl₆−Ph₄Sn as catalyst.

(3) The spacer length exerts little influence on the absorption properties of **2**(*m*). The functional bridge, however, affects the polarizability of the biphenyl mesogen, with the pendant absorption in **1**(3) being considerably blue-shifted from that of **2**(3).

(4) All the polymers are thermally stable, irrespective of the type of the functional bridge and the spacer length.

(5) While **1**(3) with the ether bridge forms SmA phase of monolayer structure, its counterpart with the ester bridge **2**(3) displays better developed mesomorphic textures, exhibits higher transition temperatures, and shows interdigitated packing arrangements of mesogenic pendants. The mesogens in the polymer with a longer spacer [**2**(4)] is, however, packed in a monolayer structure.

(6) Polymer **1**(3) is almost nonluminescent; in sharp contrast, **2**(3) is highly emissive. The emission intensity is further enhanced (almost doubled) when the spacer length is increased from 3 to 4.

The structure−property relationship gained in this study will help design liquid crystalline and light emitting polyacetylenes for high-tech applications. The efficient UV emission from the liquid crystalline polyacetylenes is of particular technological implications.[10] We are currently investigating polarized emission from the polyacetylenes **2**(*m*), in particular **2**(4), and exploring the possibility of utilizing the polymers for the construction of optical display systems with simple device configurations, high emission efficiency, and full color tunability.[20]

Experimental Section

Materials. Dioxane (Nacalai Tesque), THF (Lab-Scan), and toluene (BDH) were predried over 4 Å molecular sieves and distilled from sodium benzophenone ketyl immediately prior to use. Dichloromethane (Lab-Scan) was dried over molecular sieves and distilled over calcium hydride. 4-Pentyn-1-ol, 5-hexyn-1-ol, and 5-chloro-1-pentyne were the products of Farchan Laboratory and were used as received. Except molybdenum(V) chloride (Acros), all other reagents and solvents were purchased from Aldrich and used without further purification.

Instrumentation. The IR spectra were measured on a Perkin-Elmer 16 PC FT-IR spectrophotometer. The ¹H and ¹³C NMR spectra were recorded on a Bruker ARX 300 NMR spectrometer using chloroform-*d* as solvent and tetramethylsilane ($\delta = 0$) or chloroform (7.26) as internal reference. The UV spectra were measured on a Milton Roy Spectronic 3000 Array spectrophotometer and the molar absorptivity (ϵ) of the polymers was calculated on the basis of their monomer repeat units. The mass spectra were recorded on a Finnigan TSQ 7000 triple quadrupole mass spectrometer operating in a chemical ionization (CI) mode using methane as carrier gas. The elemental analyses were performed by M−H−W, Phoenix, AZ. The number- and weight-average molecular weights of the polymers were estimated by a Waters Associates GPC system. Degassed THF was used as eluent at a flow rate of 1.0 mL/

min. A set of monodisperse polystyrene standards covering the molecular weight range of 10^3−10^7 was used for the molecular weight calibration.

The thermal stability of the polymers was evaluated on a Perkin-Elmer TGA 7 under dry nitrogen at a heating rate of 10 °C /min. A Setaram DSC 92 was used to measure the phase transition thermograms. An Olympus BX 60 POM equipped with a Linkam TMS 92 hot stage was used to observe anisotropic optical textures. The XRD patterns were recorded on a Philips PW1830 powder diffractometer with a graphite monochromator using 1.5406 Å Cu Kα wavelength at room temperature (scanning rate, 0.05°/s; scan range, 2−30°). The polymer samples for the XRD measurements were prepared by freezing the molecular arrangements in the liquid crystalline states by liquid nitrogen as previously reported.[6−8]

Monomer Synthesis. The alkyne monomer **3**(3) was synthesized by etherization of 4′,4-biphenol with 5-chloro-1-pentyne followed by esterification of the resulting alcohol with lauric acid in the presence of DCC, TsOH, and DMAP (cf., Scheme 1). The monomers **4**(*m*) with a different functional bridge group were prepared by esterifications of 4′-hydroxy-4-biphenylcarboxylic acid with lauric acid and *n*-alkyn-1-ol. Typical synthetic procedures are given below.

5-[(4′-Hydroxy-4-biphenylyl)oxy]-1-pentyne (7). In a 1000-mL Erlenmeyer flask equipped with a condenser were dissolved 10 g (53.7 mmol) of 4,4′-biphenol and 3 g of KOH (58.8 mmol) in 400 mL of acetone/DMSO mixture (10:1 by volume) under gentle heating and stirring. To the homogeneous solution were added 5 g (53.6 mmol) of 5-chloro-1-pentyne and a catalytic amount of potassium iodide. The resulting mixture was then refluxed for 30 h. The reaction mixture was poured into 300 mL water and acidified with 15 mL of 37% hydrochloric acid. The precipitate was collected by suction filtration. The crude product was purified on a silica gel column using chloroform as eluent followed by recrystallization from toluene. White crystal was obtained in 33% yield (5 g). IR (KBr), ν (cm⁻¹): 3375 (br, OH), 3304 (s, H−C≡), 636 (m, H−C≡ bending). ¹H NMR (300 MHz, DMSO-*d*₆), δ (ppm): 9.57 (s, OH), 7.59 (d, 2H, Ar−H meta to OH), 7.50 (d, 2H, Ar−H meta to OC₅H₇), 7.07 (d, 2H, Ar−H ortho to OH), 6.94 (d, 2H, Ar−H ortho to OC₅H7), 4.14 (t, 2H, OCH₂), 2.92 (t, 1H, H−C≡), 2.44 (td, 2H, ≡C−CH₂), 1.99 (m, 2H, OCH₂C*H*₂). ¹³C NMR (75 MHz, DMSO-*d*₆), δ (ppm): 157.6 (aromatic carbon linked with OC₅H₇), 156.7 (aromatic carbon linked with OH), 131.0 (aromatic carbon para to OH), 130.9 (aromatic carbon para to OC₅H₇), 127.4 (aromatic carbons meta to OH), 127.2 (aromatic carbons meta to OC₅H₇), 115.9 (aromatic carbons ortho to OH), 115.0 (aromatic carbons ortho to OC₅H₇), 83.9 (≡C), 71.9 (OCH₂), 66.1 (HC≡), 28.0 (≡C−CH₂CH₂), 14.7 (≡C−*C*H₂).

5-{[(4′-{[(Undecyl)carbonyl]oxy})-4-biphenylyl]oxy}-1-pentyne [3(3)]. In a typical run, lauric acid (2.9 g, 14.5 mmol), 5-[(4′-hydroxy-4-biphenylyl)oxy]-1-pentyne (3.6 g, 14.3 mmol), TsOH (0.6 g, 3.5 mmol), and DMAP (0.4 g, 3.3 mmol) were dissolved in 250 mL of dry THF in a 500-mL, two-necked flask in an atmosphere of nitrogen. The solution was cooled to 0−5 °C with an ice−water bath, to which 4.6 g of DCC (22.3 mmol) dissolved in 50 mL of THF was added under stirring via a dropping funnel. The reaction mixture was stirred overnight. After the formed urea solid was filtered out, the solution was concentrated by a rotary evaporator. The product was purified by a silica gel column using chloroform as eluent. Recrystallization from absolute ethanol gave 5.0 g of white crystals (yield: 87%). IR (KBr), ν (cm⁻¹): 3300 (s, H−C≡), 1748 (vs, C=O), 630 (m, H−C≡ bending). ¹H NMR (300 MHz, CDCl₃), δ (ppm): 7.55 (d, 2H, Ar−H meta to OCO), 7.49 (d, 2H, Ar−H meta to OC₅H₇), 7.14 (d, 2H, Ar−H ortho to OCO), 6.99 (d, 2H, Ar−H ortho to OC₅H₇), 4.12 (t, 2H, OCH₂), 2.57 (t, 2H, OCOCH₂), 2.43 (td, 2H, ≡C−CH₂), 2.01 (m, 3H, HC≡ and OCH₂C*H*₂), 1.77 (m, 2H, OCOCH₂C*H*₂), 1.43−1.28 [m, 16H, (CH)₂], 0.89 (t, 3H, CH₃). ¹³C NMR (75 MHz, CDCl₃), δ (ppm): 172.4 (C=O), 158.4 (aromatic carbon linked with OC₅H₇), 149.6 (aromatic carbon linked with OCO), 138.4 (aromatic carbon para to OCO), 132.9 (aromatic carbon para to OC₅H₇), 128.0 (aromatic carbons meta to OCO), 127.6 (aromatic carbons meta

to OC$_5$H$_7$), 121.7 (aromatic carbons ortho to OCO), 114.7 (aromatic carbons ortho to OC$_5$H$_7$), 83.3 (≡C), 68.9 (OCH$_2$), 66.1 (HC≡), 34.5 (OCO*C*H$_2$), 31.9 (*C*H$_2$C$_2$H$_5$), 29.6 (OCOC$_2$H$_4$-*C*H$_2$), 29.4 (OCOC$_5$H$_{10}$*C*H$_2$), 29.3 (OCOC$_4$H$_8$*C*H$_2$ and OCOC$_6$-H$_{12}$*C*H$_2$), 29.2 (OCOC$_3$H$_6$*C*H$_2$), 29.1 (*C*H$_2$C$_3$H$_7$), 28.1 (≡C–CH$_2$*C*H$_2$), 24.9 (OCOCH$_2$*C*H$_2$), 22.7 (*C*H$_2$CH$_3$), 15.1 (≡C–*C*H$_2$), 14.1 (CH$_3$). MS (CI): *m/e* 435.3 [(*M* + 1)$^+$; calcd 435.3)]. Anal. Calcd for C$_{29}$H$_{38}$O$_3$: C; 80.13, H; 8.82. Found: C; 80.00, H; 8.49.

(4′-{[(Undecyl)carbonyl]oxy})-4-biphenylcarboxylic acid (10). Into a 100-mL, two- necked, round-bottomed flask were added 4.0 g (20 mmol) of lauric acid, 3 mL of thionyl chloride, and 20 mL of THF. After refluxing for 2 h, the excess thionyl chloride was distilled off under reduced pressure. The solid left in the flask was dissolved in 20 mL of THF and cooled using an ice bath. A solution of 4′-hydroxy-4-biphenylcarboxylic acid (4.5 g, 21 mmol) and pyridine (2 mL) in 30 mL of THF was injected into the flask, and the mixture was slowly warmed to room temperature and stirred overnight. THF was then distilled off using a rotary evaporator. Recrystallization of the solid residue from absolute ethanol gave 5.6 g of product: white crystal; yield 69.6%. IR (KBr), ν (cm^{-1}): 1746 (vs, C=O stretching in OCOC$_{11}$H$_{23}$), 1684 (vs, C=O stretching in CO$_2$H). ^{1}H NMR (300 MHz, DMSO-d_6), δ (ppm): 13.01 (s, 1H, CO$_2$H), 8.13 (d, 2H, Ar–H ortho to CO$_2$H), 7.80 (m, 4H, Ar–H), 7.30 (d, 2H, Ar–H ortho to OCOC$_{11}$H$_{23}$), 2.70 (t, 2H, OCOC*H*$_2$), 1.80 (m, 2H, OCOC*H$_2$*CH$_2$), 1.40 [m, 16H, (CH$_2$)$_8$], 1.00 (t, 3H, CH$_3$). ^{13}C NMR (75 MHz, DMSO-d_6), δ (ppm): 171.8 (O*C*OC$_{11}$H$_{23}$), 170.2 (*C*O$_2$H), 150.3 (aromatic carbon linked with OCOC$_{11}$H$_{23}$), 143.5 (aromatic carbon para to CO$_2$H), 136.6 (aromatic carbon para to OCOC$_{11}$H$_{23}$), 123.0 (aromatic carbons ortho to CO$_2$H), 129.8 (aromatic carbon linked with CO$_2$H), 128.2 (aromatic carbons meta to CO$_2$H), 126.8 (aromatic carbons meta to OCOC$_{11}$H$_{23}$), 122.5 (aromatic carbons ortho to OCOC$_{11}$H$_{23}$), 33.6 (OCO*C*H$_2$), 31.3 (*C*H$_2$CH$_2$-CH$_3$), 29.1 (OCOC$_2$H$_4$*C*H$_2$), 29.0 (OCOC$_5$H$_{10}$*C*H$_2$) 28.8 (OCO-C$_4$H$_8$*C*H$_2$ and OCOC$_6$H$_{12}$*C*H$_2$), 28.7 (OCOC$_3$H$_6$*C*H$_2$), 28.5 (*C*H$_2$CH$_3$), 24.5 (OCOCH$_2$*C*H$_2$), 22.2 (*C*H$_2$), 14.0 (CH$_3$).

5-({[(4′-{[(Undecyl)carbonyl]oxy})-4-biphenylyl]carbonyl}oxy)-1-pentyne [4(3)]. In a 500-mL, two-necked, round-bottom flask were dissolved (4′-{[(undecyl)carbonyl]-oxy})-4-biphenylcarboxylic acid (1.25 g, 3.2 mmol), 4-pentyn-1-ol (0.32 g, 3.8 mmol), DCC (0.98 g, 4.8 mmol), TsOH (0.12 g, 0.70 mmol), and DMAP (0.08 g, 0.65 mmol) in 250 mL of dry dichloromethane. After the solution was stirred for 24 h, the formed urea was filtered out and the solvent was removed by a rotary evaporator. The residue was purified by a silica gel column using dichloromethane as eluent followed by recrystallization from absolute ethanol.

Characterization Data. 4(3). White crystal; yield 74.6%. IR (KBr), ν (cm^{-1}): 3288 (s, H–C≡), 1746 (vs, C=O stretching in OCOC$_{11}$H$_{23}$), 1714 (vs, C=O stretching in CO$_2$C$_5$H$_7$), 654 (m, H–C≡ bending). ^{1}H NMR (300 MHz, CDCl$_3$), δ (ppm): 8.12 (d, 2H, Ar–H ortho to CO$_2$C$_5$H$_7$), 7.62 (d, 4H, Ar–H para to CO$_2$C$_5$H$_7$ and OCOC$_{11}$H$_{23}$), 7.21 (d, 2H, Ar–H ortho to OCOC$_{11}$H$_{23}$), 4.56 (t, 2H, CO$_2$C*H*$_2$C$_4$H$_5$), 2.58 (t, 2H, OCOC*H*$_2$-C$_{10}$H$_{21}$), 2.41 (td, 2H, ≡C–CH$_2$), 2.02 (m, 3H, ≡CCH$_2$C*H*$_2$ and HC≡), 1.78 (m, 2H, OCOCH$_2$C*H*$_2$) 1.55–1.40 [m, 16H, (CH$_2$)$_8$], 0.88 (t, 3H, CH$_3$). ^{13}C NMR (75 MHz, CDCl$_3$), δ (ppm): 172.1 (O*C*OC$_{11}$H$_{23}$), 169.3 (*C*O$_2$C$_5$H$_7$), 150.9 (aromatic carbon linked with OCOC$_{11}$H$_{23}$), 144.8 (aromatic carbon para to CO$_2$C$_5$H$_7$), 137.5 (aromatic carbon para to OCOC$_{11}$H$_{23}$), 130.1 (aromatic carbon ortho to CO$_2$C$_5$H$_7$), 129.0 (aromatic carbon linked with CO$_2$C$_5$H$_7$), 128.3 (aromatic carbons meta to CO$_2$C$_5$H$_7$), 127.0 (aromatic carbons meta to OCOC$_{11}$H$_{23}$), 122.1 (aromatic carbons ortho to OCOC$_{11}$H$_{23}$), 83.0 (≡C), 69.1 (HC≡), 63.5 (CO$_2$*C*H$_2$), 34.4 (OCO*C*H$_2$), 31.9 (*C*H$_2$C$_2$H$_5$), 29.6 (OCOC$_2$H$_4$*C*H$_2$), 29.4 (*C*H$_2$C$_5$H$_{11}$), 29.3 (OCOC$_4$H$_8$*C*H$_2$ and OCOC$_6$H$_{12}$*C*H$_2$), 29.2 (OCOC$_3$H$_6$*C*H$_2$), 29.1 (*C*H$_2$C$_3$H$_7$), 27.7 (≡C–CH$_2$*C*H$_2$), 24.9 (OCOCH$_2$*C*H$_2$), 22.6 (*C*H$_2$CH$_3$), 15.4 (≡C–*C*H$_2$), 14.0 (CH$_3$). MS (CI): *m/e* 463.3 [(*M* + 1)$^+$; calcd 463.3]. Anal. Calcd for C$_{30}$-H$_{38}$O$_4$: C, 77.88; H, 8.28. Found: C, 77.53; H, 7.85.

4(4). White crystal; yield 88.2%. IR (KBr), ν (cm^{-1}): 3256 (s, H–C≡), 1754 (vs, C=O stretching in OCOC$_{11}$H$_{23}$), 1716 (vs, C=O stretching in CO$_2$C$_6$H$_9$), 674 (m, H–C≡ bending). ^{1}H

NMR (300 MHz, CDCl$_3$), δ (ppm): 8.12 (d, 2H, Ar–H ortho to CO$_2$C$_6$H$_9$), 7.6 (m 4H, Ar–H para to CO$_2$C$_6$H$_9$ and OCOC$_{11}$H$_{23}$), 7.19 (d, 2H, Ar–H ortho to OCOC$_{11}$H$_{23}$), 4.37 (t, 2H, CO$_2$C*H$_2$*-C$_5$H$_7$), 2.58 (t, 2H, OCOC*H*$_2$), 2.30 (td, 2H, ≡C–CH$_2$), 1.98 (t, 1H, HC≡), 1.93 (m, 2H, OCOCH$_2$C*H$_2$*), 1.75 (m, 4H, OCOCH$_2$-C*H*$_2$ and ≡CCH$_2$C*H*$_2$), 1.27 [m, 16H, (CH$_2$)$_8$], 0.88 (t, 3H, CH$_3$). ^{13}C NMR (75 MHz, CDCl$_3$), δ (ppm): 172.3 (O*C*O C$_{11}$H$_{23}$), 166.4 (*C*O$_2$C$_6$H$_9$), 150.9 (aromatic carbon linked with OCO C$_{11}$H$_{23}$), 144.8 (aromatic carbons para to CO$_2$C$_6$H$_9$), 134.6 (aromatic carbon para to OCOC$_{11}$H$_{23}$), 130.1 (aromatic carbons ortho to CO$_2$C$_6$H$_9$), 129.2 (aromatic carbon linked with CO$_2$C$_6$H$_9$), 128.3 (aromatic carbons meta to CO$_2$C$_6$H$_9$), 127.0 (aromatic carbons meta to OCOC$_{11}$H$_{23}$), 122.1 (aromatic carbons ortho to OCOC$_{11}$H$_{23}$), 83.9 (≡C), 68.8 (HC≡), 64.5 (CO$_2$*C*H$_2$C$_5$H$_7$), 34.3 (OCO*C*H$_2$), 31.9 (OCOC$_8$H$_{16}$*C*H$_2$), 29.6 (OCOC$_2$H$_4$*C*H$_2$), 29.5 (OCO$_2$CH$_2$*C*H$_2$), 29.3 (OCOC$_5$H$_{10}$*C*H$_2$), 29.2 (OCOC$_4$H$_8$*C*H$_2$), 29.1 (OCOC$_3$H$_6$*C*H$_2$), 27.8 (OCO $_2$C$_7$H$_{14}$*C*H$_2$), 25.1 (≡C–CH$_2$*C*H$_2$), 25.0 (OCOCH$_2$*C*H$_2$), 22.7 (*C*H$_2$CH$_3$), 17.5 (≡C–*C*H$_2$), 14.1 (CH$_3$). MS (CI): *m/e* 477.3 [(*M* + 1)$^+$; calcd 477.3]. Anal. Calcd for C$_{31}$H$_{40}$O$_4$: C, 78.10; H, 8.46. Found: C, 78.24; H, 8.32.

Polymerization. All the polymerization reactions and manipulations were carried out under nitrogen using Schlenk techniques in a vacuum line system or an inert-atmosphere glovebox (Vacuum Atmospheres), except for the purification of the polymers, which was done in an open atmosphere. A typical experimental procedure for the polymerization of **3**(3) is given below.

Into a baked 20 mL Schlenk tube with a stopcock in the sidearm was added 375.0 mg (0.8 mmol) of **3**(3). The tube was evacuated under vacuum and then flushed with dry nitrogen three times through the sidearm. Freshly distilled 1,4-dioxane (2 mL) was injected into the tube to dissolve the monomer. The catalyst solution was prepared in another tube by dissolving 16.0 mg of tungsten(VI) chloride and 17.0 mg of tetraphenyltin in 2 mL of 1,4-dioxane. The two tubes were aged at 60 °C for 15 min and the monomer solution was transferred to the catalyst solution using a hypodermic syringe. The reaction mixture was stirred at room temperature under nitrogen for 24 h. The solution was then cooled to room temperature, diluted with 5 mL of chloroform, and added dropwise to 500 mL of acetone through a cotton filter under stirring. The precipitate was allowed to stand overnight, which was then filtered with a Gooch crucible. The polymer was washed with acetone and dried in a vacuum oven to a constant weight.

Characterization Data. 1(3). Red powdery solid; yield 68.9%. M_w 9750; M_w/M_n 1.78 (GPC; Table 2, no. 11). IR (KBr), ν (cm^{-1}): 1756 (vs, C=O). ^{1}H NMR (300 MHz, CDCl$_3$), δ (ppm): 7.35, 7.00, 6.82 (Ar–H and trans H–C=), 6.14 (cis H–C=), 3.87 (OCH$_2$), 2.56 (OCOCH$_2$), 2.1 (=C–CH$_2$), 1.81 (OCOCH$_2$C*H*$_2$), 1.35 [(CH$_2$)$_9$], 0.96 (CH$_3$). ^{13}C NMR (75 MHz, CDCl$_3$), δ (ppm): 172.1 (C=O), 158.5 (aromatic carbon linked with OC$_5$H$_7$), 149.7 (aromatic carbon linked with OCOC$_{11}$H$_{23}$), 138.0 (aromatic carbon para to OCOC$_{11}$H$_{23}$), 132.5 (aromatic carbon para to OC$_5$H$_7$), 127.9 (aromatic carbons meta to OCOC$_{11}$H$_{23}$), 127.4 (aromatic carbons meta to OC$_5$H$_7$), 121.8 (aromatic carbons ortho to OCOC$_{11}$H$_{23}$), 114.7 (aromatic carbons ortho to OC$_5$H$_7$), 67.4, (OCH$_2$), 34.4 (OCO*C*H$_2$ and =C–CH$_2$), 31.9 (*C*H$_2$C$_2$H$_5$), 29.7 (OCOC$_2$H$_4$*C*H$_2$), 29.4 (OCOC$_5$-H$_{10}$*C*H$_2$, OCOC$_4$H$_8$*C*H$_2$, OCOC$_6$H$_{12}$*C*H$_2$ and OCOC$_3$H$_6$*C*H$_2$), 29.2 (OCOC$_3$H$_6$*C*H$_2$ and *C*H$_2$C$_3$H$_7$), 25.0 (OCOCH$_2$*C*H$_2$), 22.7 (*C*H$_2$CH$_3$), 14.1 (CH$_3$). UV (CHCl$_3$, 1.13 × 10^{-4} mol /L), λ_{max} (nm)/ϵ_{max} (mol^{-1} L cm^{-1}): 265/2.23 × 10^4, 360 (sh)/1.33 × 10^3.

2(3). Yellow powdery solid; yield 84.1%. M_w 37 700; M_w/M_n 1.9 (GPC, Table 3, no. 3). IR (KBr), ν (cm^{-1}): 1758 (C=O stretching in OCOC$_{11}$H$_{23}$), 1716 (C=O stretching in CO$_2$C$_5$H$_7$). ^{1}H NMR (300 MHz, CDCl$_3$), δ (ppm): 7.93, 7.39, 6.97 (Ar–H and trans H–C=), 5.96 (cis H–C=), 4.32 (CO$_2$CH$_2$), 2.59 (OCOCH$_2$), 2.06 (=C–CH$_2$), 1.80 (OCOCH$_2$C*H*$_2$ and =C–CH$_2$C*H*$_2$), 1.36 [(CH$_2$)$_8$], 0.96 (CH$_3$). ^{13}C NMR (75 MHz, CDCl$_3$), δ (ppm): 171.8 (O*C*OC$_{11}$H$_{23}$), 165.9 (*C*O$_2$C$_5$H$_7$), 150.5 (aromatic carbon linked with OCOC$_{11}$H$_{23}$), 144.0 (aromatic carbon para to CO$_2$C$_5$H$_7$), 137.1 (aromatic carbon para to OCOC$_{11}$H$_{23}$), 129.9 (aromatic carbons ortho to CO$_2$C$_5$H$_7$), 128.8 (aromatic carbon

linked with $CO_2C_5H_7$), 128.0 (aromatic carbons meta to $CO_2C_5H_7$), 126.8 (aromatic carbons meta to $OCOC_{11}H_{23}$), 121.8 (aromatic carbons ortho to $OCOC_{11}H_{23}$), 64.3 (CO_2CH_2), 34.3 ($OCOCH_2$ and $=C-CH_2$), 31.8 ($CH_2C_2H_5$), 29.6 ($OCOC_2H_4CH_2$), 29.5 ($OCOC_5H_{10}CH_2$), 29.3 ($OCOC_4H_8CH_2$ and $OCOC_6H_{12}CH_2$), 29.1 ($OCOC_3H_6CH_2$ and $OCOC_7H_{14}CH_2$), 24.8 ($OCOCH_2CH_2$), 22.6 (CH_2CH_3), 14.0 (CH_3). UV ($CHCl_3$, 9.00×10^{-5} mol/L), $\lambda_{max}/\epsilon_{max}$: 277 nm/$2.56 \times 10^4$ mol^{-1} L cm^{-1}.

2(4). Red powdery solid; yield 82.3%. M_w 59 000, M_w/M_n 1.85 (GPC; Table 4, no. 3). IR (KBr), ν (cm^{-1}): 1756 (vs, $C=O$ stretching in $OCOC_{11}H_{23}$), 1716 (vs, $C=O$ stretching in $CO_2C_6H_9$). ^{1}H NMR (300 MHz, CDCl$_3$), δ (ppm): 7.87, 7.35, 6.97 (Ar–H and trans H–C=), 5.75 (cis H–C=), 4.22 (CO_2CH_2), 2.34 ($OCOCH_2$), 2.06 ($=C-CH_2$), 1.71–1.27 [$(CH_2)_{12}$], 0.88 (CH_3). ^{13}C NMR (75 MHz, CDCl$_3$), δ (ppm): 171.9 ($OCOC_{11}H_{23}$), 166.0 ($CO_2C_6H_9$), 150.7 (aromatic carbon linked with OCO-$C_{11}H_{23}$), 144.7 (aromatic carbon para to $CO_2C_6H_9$), 137.7 (aromatic carbon para to $OCOC_{11}H_{23}$), 129.9 (aromatic carbons ortho to $CO_2C_6H_9$), 129.0 (aromatic carbon linked with $CO_2C_6H_9$), 128.1 (aromatic carbons meta to $CO_2C_6H_9$), 126.7 (aromatic carbons meta to $OCOC_{11}H_{23}$), 121.9 (aromatic carbons ortho to $OCOC_{11}H_{23}$), 64.8 (CO_2CH_2), 34.3 ($OCOCH_2$ and $=C-CH_2$), 31.9 ($CH_2C_2H_5$), 29.6 ($OCOC_2H_4CH_2$), 29.5 ($OCO-CH_2CH_2$), 29.3 ($OCOC_5H_{10}CH_2$), 29.2 ($OCOC_4H_8CH_2$ and $OCOC_3H_6CH_2$), 24.9 ($OCOCH_2CH_2$), 22.7 (CH_2CH_3), 14.1 (CH_3). UV (CHCl$_3$, 8.80×10^{-5} mol/L), $\lambda_{max}/\epsilon_{max}$: 276 nm/$2.34 \times 10^4$ mol^{-1} L cm^{-1}.

References and Notes

(1) For selected examples of reviews and monographs, see: (a) *Liquid Crystalline Polymer Systems*; Isayev, A. I., Kyu, T., Cheng, S. Z. D., Eds.; American Chemical Society: Washington, DC, 1996. (b) Mao, G.; Ober, C. K. *Acta Polym.* **1997**, *48*, 405. (c) Pugh, C.; Kiste, A. L. *Prog. Polym. Sci.* **1997**, *22*, 601. (d) Hsu, C. S. *Prog. Polym. Sci.* **1997**, *22*, 829. (e) Percec, V.; Tomazos, D. *Adv. Mater.* **1992**, *4*, 548. (f) Percec, V.; Tomazos, D. In *Comprehensive Polymer Science*, 1st Supplement; Aggarwal, S. L., Russo, S., Eds.; Pergamon: Oxford, England, 1992; Chapter 14, pp 299−383. (g) *Liquid Crystal Polymers: from Structures to Applications*; Collyer, A. A., Ed.; Elsevier Applied Science: New York, 1992. (h) Percec, V.; Pugh, C. In *Side Chain Liquid Crystal Polymers*; McArdle, C. B., Ed.; Chapman & Hall: New York, 1989; Chapter 3, pp 30−105.

(2) (a) Akagi, K.; Shirakawa, H. *Macromol. Symp.* **1996**, *104*, 137. (b) Choi, S. K.; Lee, J. H.; Kang, S. J.; Jin, S. H. *Prog. Polym. Sci.* **1997**, *22*, 693. (c) Choi, S. K.; Gal, Y. S.; Jin, S. H.; Kim, H. K. *Chem. Rev.* **2000**, *100*, 1645.

(3) (a) Dai, X. M.; Goto, H.; Akagi, K,; Shirakawa, H. *Synth. Met.* **1999**, *103*, 1289. (b) Lino, K.; Goto, H.; Akagi, K.; Shirakawa, H.; Kawaguchi, A. *Synth. Met.* **1997**, *84*, 967. (c) Yoshino, K.; Kobayashi, K.; Myofin, K, Ozaki, M.; Akagi, K.; Goto, H.; Shirakawa, H. *Jpn. Appl. Phys.* **1996**, *35*, 3964. (d) Akagi, K.; Goto, H.; Iino, K.; Shirakawa, H.; Isoya, J. *Mol. Cryst. Liq. Cryst.* **1995**, *267*, 277. (e) Shirakawa, H.; Kadokura, Y.; Goto, H.; Oh, S.-Y.; Akagi, K.; Araya, K. *Mol. Cryst. Liq. Cryst.* **1994**, *255*, 213. (f) Oh, S.-Y.; Akagi, K.; Shirakawa, H.; Araya, K. *Macromolecules* **1993**, *26*, 620.

(4) (a) Koltzenburg, S.; Stelzer, F.; Nuyken, O. *Macromol. Chem. Phys.* **1999**, *200*, 821. (b) Koltzenburg, S.; Ungerank, M.; Stelzer, F.; Nuyken, O. *Macromol. Chem. Phys.* **1999**, *200*, 814. (c) Koltzenburg, S.; Wolff, P.; Stelzer, F.; Springer, J.; Nuyken, O. *Macromolecules* **1998**, *31*, 9166.

(5) (a) Tang, B. Z. *Polym. News* **2001**, *26*, 262. (b) Xu, K.; Peng, H.; Lam, J. W. Y.; Poon, T. W. H.; Dong, Y.; Xu, H.; Sun, Q.; Cheuk, K. K. L.; Salhi, F.; Lee, P. P. S.; Tang, B. Z. *Macromolecules* **2000**, *33*, 6918. (c) Tang, B. Z.; Kong, X.; Wan, X.; Peng, H.; Lam, J. W. Y.; Feng, X.; Kwok, H. S. *Macromolecules* **1998**, *31*, 2419. (d) Tang, B. Z.; Kong, X.; Wan, X.; Feng, X.-D. *Macromolecules* **1997**, *30*, 5620.

(6) (a) Mi, Y. L.; Tang, B. Z. *Polym. News* **2001**, *26*, 170. (b) Tang, B. Z.; Lam, J. W. Y.; Kong, X.; Salhi, F.; Cheuk, K. K. L.; Kwok, H. S.; Huang, Y. M.; Ge, W. In *Liquid Crystals IV*; Khoo, I., Ed.; SPIE-The International Society for Optical Engineering: Bellingham, WA, 2000; pp 24−30. (c) Kong, X.; Lam, J. W. Y.; Tang, B. Z. *Macromolecules* **1999**, *32*, 1722.

(7) (a) Kong, X.; Tang, B. Z. *Chem. Mater.* **1998**, *10*, 3352. (b) Tang, B. Z.; Lam, J. W. Y., Kong, X.; Lee, P. P. S.; Wan, X.; Kwok, H. S.; Huang, Y. M.; Ge, W.; Chen, H.; Xu, R.; Wang, M. In *Liquid Crystals III*; Khoo, I., Ed.; SPIE-The International Society for Optical Engineering: Bellingham, WA, 1999; pp 62−71.

(8) Lam, J. W. Y.; Kong, X.; Dong, Y. P.; Cheuk, K. K. L.; Xu, K.; Tang, B. Z. *Macromolecules* **2000**, *33*, 5027.

(9) Huang, Y. M.; Ge, W.; Lam, J. W. Y.; Tang, B. Z. *Appl. Phys. Lett.* **2001**, *78*, 1652.

(10) (a) Qiu, C. F.; Wang, L. D.; Chen, H. Y.; Wong, M.; Kwok, H. S. *Appl. Phys. Lett.* **2001**, *79*, 2276. (b) Tao, Y. T.; Balasubramaniam, E.; Danel, A.; Tomasik, P. *Appl. Phys. Lett.* **2000**, *77*, 933. (c) Kajima, Y.; Asai, N.; Tamura, S. *Jpn. Appl. Phys. Part 1* **1999**, *38*, 5274. (d) Yuan, C. H.; Hoshina, S.; Toyoda, S.; Suzuki, H.; Fujiki, M.; Matsumoto, N. *Appl. Phys. Lett.* **1997**, *71*, 3326. (e) Tang, C. W.; Williams, D. J.; Chang, J. C. U.S. Patent 5 294 870, 1994.

(11) (a) Lauchlan, L.; Etemad, S.; Chung, T.-C.; Heeger, A. J.; MacDiarmid, A. G. *Phys. Rev. B* **1981**, *24*, 3701. (b) Yoshino, K.; Hayashi, S.; Inuishi, Y.; Hattori, K.; Watanabe, Y. *Solid State Commun.* **1983**, *46*, 583. (c) Carter, P. W.; Porter, J. D. *Phys. Rev. B*, **1991**, *43*, 14478. (d) Friend, R. H.; Gymer, R. W.; Holms, A. B.; Burroughes, J. H.; Marks, R. N.; Taliani, C.; Bradley, D. D. C.; Dos Santos, D. A.; Brédas, J. L.; Lögdlund, M.; Salaneck, W. R. *Nature*, **1999**, *397*, 121.

(12) (a) Fujii, A.; Hidayat. R.; Sonoda, T.; Fujisawa, T.; Ozaki, M.; Vardeny, Z. V.; Teraguchi, M.; Masuda, T.; Yoshino, K. *Synth. Met.* **2001**, *116*, 95. (b) Hidayat, R.; Tatsuhara, S.; Kim, D. W.; Ozaki, M.; Yoshino, K.; Teraguchi, M.; Masuda, T. *Phys. Rev. B* **2000**, *61*, 10167. (c) Hidayat, R.; Hirohata, M.; Tatsuhara, S.; Ozaki, M.; Teraguchi, M.; Masuda, T.; Yoshino, K. *Synth. Met.* **1999**, *101*, 210. (d) Frolov, S. V.; Fujii, A.; Chinn, D.; Hirohata, M.; Hidayat, R.; Taraguchi, M.; Masuda, T.; Yoshino, K.; Vardeny, Z. V. *Adv. Mater.* **1998**, *10*, 869. (e) Yoshino, K.; Hirohata, M.; Hidayat, R.; Tada, K.; Sada, T.; Teraguchi, M.; Masuda, T.; Frolov, S. V.; Shkunov, M.; Vardeny, Z. V.; Hamaguchi, M. *Synth. Met.* **1997**, *91*, 283.

(13) (a) Sun, R. G.; Zheng, Q. B.; Zhang, X. M.; Masuda, T.; Kobayashi, T. *Jpn. J. Appl. Phys.* **1999**, *38*, 2017. (b) Sun, R. G.; Masuda, T.; Kobayashi, T. *Synth. Met.* **1997**, *91*, 301. (c) Sun, R. G.; Masuda, T.; Kobayashi, T. *Jpn. J. Appl. Phys.* **1996**, *35*, L1673. (d) Sun, R. G.; Masuda, T.; Kobayashi, T. *Jpn. J. Appl. Phys.* **1996**, *35*, L1434.

(14) (a) Huang, Y. M.; Lam, J. W. Y.; Cheuk, K. K. L.; Ge, W.; Tang, B. Z. *Macromolecules* **1999**, *32*, 5976. (b) Huang, Y. M.; Ge, W.; Lam, J. W. Y.; Tang, B. Z. *Appl. Phys. Lett.* **1999**, *75*, 4094. (c) Lee, P. P. S.; Geng, Y. H.; Kwok, H. S.; Tang, B. Z. *Thin Solid Films* **2000**, *363*, 149. (d) Huang, Y. M.; Lam, J. W. Y.; Cheuk, K. K. L.; Ge, W.; Tang, B. Z. *Thin Solid Films* **2000**, *363*, 146. (e) Huang, Y. M.; Ge, W.; Lam, J. W. Y.; Cheuk, K. K. L.; Tang, B. Z. *Mater. Sci. Eng. B* **2001**, *85*, 242. (f) Huang, Y. M.; Ge, W.; Lam, J. W. Y.; Cheuk, K. K. L.; Tang, B. Z. *Mater. Sci. Eng. B* **2001**, *85*, 122. (g) Huang, Y. M.; Ge, W.; Lam, J. W. Y.; Cheuk, K. K. L.; Tang, B. Z. *Mater. Sci. Eng. B* **2001**, *85*, 118.

(15) (a) Gray, G. W.; Goodby, J. W. G. *Smectic Liquid Crystals: Texture and Structures*; Leonard Hill: London, 1984. (b) Demus, D.; Richter, L. *Textures of Liquid Crystals*; Verlag Chemie: Weinheim, Germany, 1978. (c) Cowie, J. M. G. *Polymers: Chemistry & Physics of Modern Materials*, 2nd ed.; Blackie Academic & Professional: London, 1991.

(16) (a) Imrie, C. T.; *Struct. Bonding* **1999**, *95*, 149. (b) Imrie, C. T.; Karasz, F. E.; Attard, G. S. *Macromolecules* **1993**, *26*, 545.

(c) Imire, C. T.; Schleen, T.; Karasz, F. E.; Attard, G. S. *Macromolecules* **1993**, *26*, 539.

(17) Okano, Y.; Masuda, T.; Higashimura, T. *J. Polym. Sci., Polym. Chem. Ed.* **1985**, *23*, 2637.

(18) (a) Masuda, T.; Okano, Y.; Tamura, K.; Higashimura, T. *Polymer* **1985**, *26*, 793. (b) Masuda, T.; Tang, B. Z.; Higashimura, T.; Yamaoka, H. *Macromolecules* **1985**, *18*, 2369.

(19) Mariani, P.; Rustichelli, F.; Torquati, G. In *Physics of Liquid Crystalline Materials*; Khoo, I.-C., Simoni, F., Eds.; Gordon & Breach Science: New York, 1991; Chapter 1.

(20) (a) Xie, Z. L.; Lam, J. W. Y.; Qiu, C. F.; Luo, J. D.; Tang, B. Z.; Kwok, H. S. *Asia Display/IDW'01* **2001**, 1451. (b) Tang, B. Z.; Lam, J. W. Y.; Luo, J, D.; Dong, Y.; Cheuk, K. K. L.; Xie, Z.; Kwok, H.-S. In *Liquid Crystals V*; Khoo, I., Ed.; SPIE-The International Society for Optical Engineering: Bellingham, WA, in press.